



**HAL**  
open science

## A Simple Model of Non-Spiking Neurons

Loïs Naudin, Juan Luis Jiménez Laredo, Nathalie Corson

► **To cite this version:**

Loïs Naudin, Juan Luis Jiménez Laredo, Nathalie Corson. A Simple Model of Non-Spiking Neurons. 2022. hal-03705452

**HAL Id: hal-03705452**

**<https://hal.science/hal-03705452>**

Preprint submitted on 27 Jun 2022

**HAL** is a multi-disciplinary open access archive for the deposit and dissemination of scientific research documents, whether they are published or not. The documents may come from teaching and research institutions in France or abroad, or from public or private research centers.

L'archive ouverte pluridisciplinaire **HAL**, est destinée au dépôt et à la diffusion de documents scientifiques de niveau recherche, publiés ou non, émanant des établissements d'enseignement et de recherche français ou étrangers, des laboratoires publics ou privés.

# A Simple Model of Non-Spiking Neurons

Loïs Naudin<sup>1\*</sup>, Juan Luis Jiménez Laredo<sup>2</sup>, and Nathalie Corson<sup>1</sup>

<sup>1</sup>Normandie Univ, UNIHAVRE, Laboratory of Applied Mathematics,  
FR-CNRS-3335, ISCN, Le Havre, 76600, France

<sup>2</sup>Normandie Univ, UNIHAVRE, Laboratory of Computer Sciences,  
FR-CNRS-3638, ISCN, Le Havre, 76600, France

\*Corresponding author: lois.naudin@gmail.com

June 27, 2022

## Abstract

Due to the ubiquity of spiking neurons in neuronal processes, various simple spiking neuron models have been proposed as an alternative to conductance-based models (a.k.a. Hodgkin–Huxley type models), known to be computationally expensive and difficult to treat mathematically. However, to the best of our knowledge, there is no equivalent in the literature of a simple and lightweight model for describing the voltage behavior of non-spiking neurons, which also are ubiquitous in a large variety of nervous tissues in both vertebrate and invertebrate species, and play a central role in information processing. This paper proposes a simple model that reproduces the experimental qualitative behavior of known types of non-spiking neurons. The proposed model, which differs fundamentally from classic simple spiking models unable to characterize non-spiking dynamics due to their intrinsic structure, is derived from the bifurcation study of conductance-based models of non-spiking neurons. Since such neurons display a high sensitivity to noise, the model aims at capturing the experimental distribution of single neuron responses rather than perfectly replicating a single given experimental voltage

trace. We show that such a model: (i) can be used as a building block for realistic simulations of large non-spiking neuronal networks, and (ii) is endowed with generalization capabilities, granted by design.

**Keywords:** Neuron model; non-spiking neurons; bifurcation; *Caenorhabditis elegans*; retina.

## 1 Introduction

Conductance-based models (CBMs), based on the Hodgkin–Huxley formalism postulated in the 1950s (Hodgkin & Huxley, 1952), are an accurate biophysical representation of the neuron in which every individual parameter and state variable have an established electrophysiological meaning. Accordingly, such models have become one of the most powerful computational approaches for understanding ‘low-level’ functions of neural systems (O’Leary et al., 2015). For instance, a CBM can describe the effect of specific conductance variations on hippocampal rhythms (Aussel et al., 2018; Giovannini et al., 2017) or predict important dendritic effects on neuronal processing (Poirazi & Papoutsis, 2020). On the downside, however, such models are computationally expensive so that one can only simulate a handful of neurons in real time (Izhikevich, 2004). Additionally, the insights obtained from a mathematical analysis perspective are quite limited as these are high-dimensional systems, difficult to treat mathematically. Therefore, to study ‘higher-level’ functions of neural systems, independent of ‘low-level’ details—be it at the level of dendrite, neuron or neural circuit (Marín et al., 2020; Shiau & Buhry, 2019)—various simple and computationally efficient models of spiking neurons have then been proposed. Some examples are the FitzHugh–Nagumo (FitzHugh, 1961), Hindmarsh–Rose (Rose & Hindmarsh, 1989), Izhikevich (Izhikevich, 2003) or various flavors of integrate-and-fire models (Górski et al., 2021; Izhikevich, 2001; Latham et al., 2000; Smith et al., 2000).

Spiking neurons are often considered as the major information processing unit of the nervous system. Nonetheless, a large variety of nervous tissues in both vertebrate and invertebrate species have revealed that a number of sensory, inter- and motor neurons function without eliciting spikes. While spiking neurons compress continuous inputs into digital signals for transmitting information via action potentials, non-spiking neurons do not elicit action potentials and modulate analog signals through graded potential responses (Lockery et al., 2009). Some examples are the invertebrate and vertebrate retinal neurons (Field & Chichilnisky, 2007), interneurons in insects and crustaceans (Roberts & Bush, 1981), motoneurons of the *Ascaris* worm (Davis & Stretton, 1989), or most of the *C. elegans* neurons (Goodman et al., 1998). Importantly, they have been found in sensorimotor and central pattern generator circuits, proven to be central in neuronal integration (Roberts & Bush, 1981) and shown to provide a determining mechanism for the control of motor behavior (Burrows et al., 1988; Laurent & Burrows, 1989a; Laurent & Burrows, 1989b).

The omnipresence and the importance of non-spiking neurons in numerous neuronal processes justify the need for a simple model capable of characterizing their behavior. To that end, Kuramochi and Doi (2017) proposed a simple model that describes the intracellular calcium dynamics of a non-spiking *C. elegans* neuron. With respect to voltage dynamics, classic simple spiking models are unfortunately unable to produce adequate non-spiking dynamics due to the topology of their phase space. In this paper, we present a simple suitable model derived from the bifurcation study of non-spiking conductance-based models, extensively used to characterize such behaviors (Kamiyama et al., 2009; Kourennyi et al., 2004; Naudin et al., 2020; Naudin et al., 2022; Nicoletti et al., 2019; Publico et al., 2006), which is able to qualitatively reproduce the two standard voltage dynamics of non-spiking neurons: *near-linear* and *bistable*. The near-linear behavior is defined by a smooth depolarization or hyperpolarization from the resting potential, while the bistable one is characterized by nonlinear transitions between the resting potential and a depolarized potential.

In order to analyze the viability and accuracy of the approach in a realistic setting,

the proposed model is used in the modeling of three non-spiking neurons of the nematode *Caenorhabditis elegans* (*C. elegans*), a well-known model organism in neuroscience (Brenner, 1974; Izquierdo, 2019; Sarma et al., 2018), that predominantly transmit information through non-spiking signals (Goodman et al., 1998). In particular, we focus on the modeling of the RIM, AIY and AFD neurons which represent, to date, the three possible forms of non-spiking neuronal responses of *C. elegans* (Figure 1). More specifically, RIM and AIY neurons display a near-linear behavior (Figure 1.A). While AIY is more sensitive to hyperpolarization than depolarization inputs with a transition point around  $-30$  mV, RIM is depolarized or hyperpolarized in a smooth manner due to the lack of large sustained currents. Finally, AFD exhibits a bistable behavior with large sustained currents restricting its membrane potential to two plateaus around  $-80$  mV and  $-15$  mV over a range of current injections (Figure 1.B).

Finally, we compare the computational efficiency of the proposed model with respect to conductance-based models developed in Naudin et al. (2020) for the same RIM, AIY and AFD neurons, as well as many additional neuron models. In particular, we show that the computational efficiency of the proposed model is of the same order of magnitude as the integrate-and-fire and Izhikevich models that are the most computational efficient neuron models to date (Izhikevich, 2003).

## 2 Proposed model

The goal of a neuronal model is to be able to reproduce the electrophysiological behavior of the neuron. To that end, it is crucial to capture its right underlying bifurcation structure (Izhikevich, 2007): the bifurcation structure describes the qualitative changes that the neuron undergoes when parameter values change. Classic simple spiking models, such as the FitzHugh–Nagumo (FitzHugh, 1961), Hindmarsh–Rose (Rose & Hindmarsh, 1989), or Izhikevich (Izhikevich, 2003) ones are specifically built on the basis of the bifurcation structure of spiking neurons. These display Andronov–Hopf bifurcations or saddle-node bifurcations

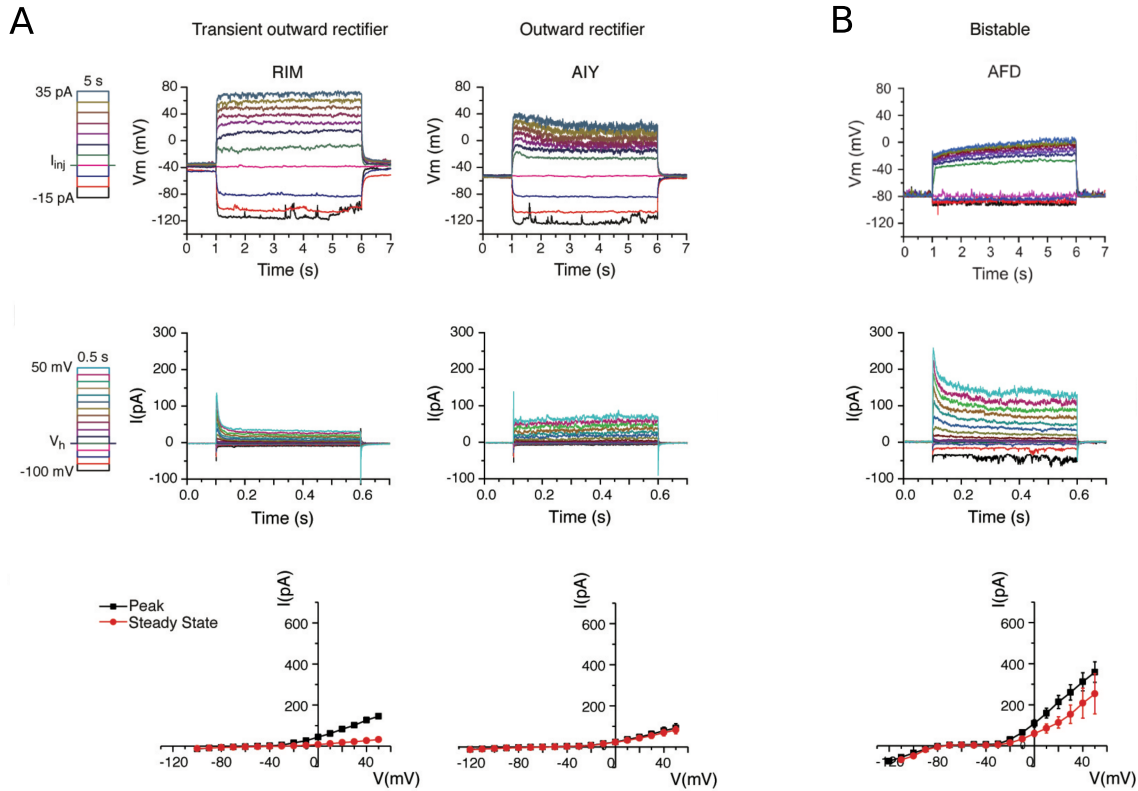


Figure 1: In-vivo recordings of three different non-spiking neurons of *C. elegans* which represent, to date, the three forms of possible non-spiking neuronal responses of the nematode. (Top) Example of the evolution of membrane potential for a series of current injections, in the space of 5 seconds, starting from  $-15$  pA and increasing to 35 pA by 5 pA increments. (Middle) Example of the evolution of the total ion currents of the different neurons when their membrane potentials are clamped at a fixed value, in spans of 0.5 seconds, from  $-100$  mV and increasing to 50 mV by 10 mV increments. (Bottom) I-V relationships obtained from averaged voltage-clamp recordings (RIM:  $n = 3$ ; AIY:  $n = 7$ ; AFD:  $n = 3$ ). Peak currents are measured by the absolute maximum amplitude of currents within the first 100 ms of each voltage step onset, while steady-state currents are measured by the averaged currents of the last 50 ms of each voltage step. **(A)** Near-linear neuron behavior with monotonic steady-state current. **(B)** Bistable neuron behavior with a N-shaped steady-state current. The figure has been reproduced from Naudin et al. (2022) with the consent of the authors.

responsible for spikes, and are therefore inherently unable to correctly characterize the dynamics of non-spiking neurons. Moreover, for the sake of completeness, we have tested the leaky integrate-and-fire model designed with a threshold high enough to avoid the triggering of spikes, as in Strohmer et al. (2021). This model is also unable to correctly characterize non-spiking dynamics (Figure S1). Such a result is expected because of the linear model employed, since the neuron dynamics are non-linear. Then, this section presents a simple model specifically derived from bifurcation studies of conductance-based models of non-spiking neurons (Naudin et al., 2021; Naudin et al., 2022) that is capable of reproducing their qualitative dynamics.

**Conductance-based models (CBMs).** In CBMs, the dynamics of the membrane potential  $V$  is described by a general equation of the form

$$C \frac{dV}{dt} = - \sum_{ion} I_{ion} + I \quad (1)$$

where  $C$  is the membrane capacitance,  $\sum_{ion} I_{ion}$  is the total current flowing across the cell membrane, and  $I$  is an applied current. The currents  $I_{ion}$  take the form

$$I_{ion} = g_{ion} m_{ion}^a h_{ion}^b (V - E_{ion})$$

where  $m$  ( $h$ ) denotes the probability for an activation (inactivation) gate to be in the open state;  $a$  and  $b$  are the number of activation and inactivation gates, respectively;  $g_{ion}$  is the maximal conductance associated with  $ion$ ; and  $E_{ion}$  is the reversal potential.

**Bifurcation dynamics of non-spiking CBMs.** In non-spiking CBMs (Kourennyi et al., 2004; Naudin et al., 2021; Naudin et al., 2020; Nicoletti et al., 2019), the steady-state current curve  $I_\infty$  determines the number of equilibria of the system and their values, as well as the bifurcations of the resting state along with the values to which they occur. It takes the

general form

$$I_\infty(V) = \sum_{ion} I_{ion\infty}(V) \quad \text{where} \quad I_{ion\infty}(V) = g_{ion} m_{ion\infty}^a(V) h_{ion\infty}^b(V) (V - E_{ion}) \quad (2)$$

with

$$x_\infty(V) = \frac{1}{1 + \exp\left(\frac{V_{1/2}^x - V}{k_x}\right)}, \quad x \in \{m, h\}.$$

where  $V_{1/2}^x$  and  $k_x$  are constant parameters.

Any stationary point of gating variables  $x \in \{m, h\}$  must satisfy  $x_* = x_\infty(V_*)$ . Replacing this into the first equation on  $V$ , fixed points  $V_*$  of such models satisfy the equation

$$I_\infty(V_*) = I. \quad (3)$$

In other words, equilibria  $V_*$  correspond to the intersection between the steady-state curve  $I_\infty$  and a horizontal line  $I = c$  where  $c$  is a constant. There are two standard steady-state curves  $I_\infty$ , monotonic and cubic (Figure 2), each involving fundamentally different neuro-computational properties for non-spiking neurons:

- As shown in Figure 2.A, CBMs with a monotonic steady-state current only have one equilibrium for any value of  $I$ . This unique equilibrium is stable for non-spiking CBMs (see Naudin et al. (2021) for rigorous mathematical proofs). Thus, non-spiking neurons with such a steady-state current display a near-linear behavior characterized by smooth depolarizations or hyperpolarizations from the resting potential, such as the RIM and AIY neurons (Figure 1.A).
- As shown in Figure 2.B, a N-shaped curve leads to a saddle-node bifurcation. When  $I = c_2$ , there are 3 equilibria, noted  $V_{1*}^{c_2}$ ,  $V_{2*}^{c_2}$  and  $V_{3*}^{c_2}$ . Increasing  $I$  results in coalescence of two equilibria (the stable  $V_{1*}^{c_2}$  with the unstable  $V_{2*}^{c_2}$ ). The value  $I = c_3$ , at which the equilibria coalesce, is called the *bifurcation value*. For this value of  $I$ , there



exist 2 equilibria. For any value of  $I > c_3$ , the system has only one equilibrium (*e.g.*  $I = c_4$  or  $I = c_5$ ), that is stable (Naudin et al., 2021). In summary, when the parameter  $I$  increases, a stable and an unstable equilibrium approach, coalesce, and then annihilate each other. Non-spiking neurons with an N-shaped steady-state current display a bistable behavior characterized by a voltage jump between the resting potential and a depolarized potential of higher voltage, such as the AFD neuron (Figure 1.B).

Based on previous properties, it can be stated that the steady-state current determines the bifurcation structure of non-spiking neurons and the equilibrium values of their graded responses to particular stimuli.

**The proposed model.** Let  $V$  represent the membrane potential of a neuron. We propose the following 1-D model of the general form

$$\tau \frac{dV}{dt} = -f(V) + I \quad (4)$$

with  $f$  a cubic function which reads as

$$f(V) = aV^3 + bV^2 + cV + d. \quad (5)$$

The function  $f$  plays the same role in the dynamics of the model (4) as the steady-state current  $I_\infty$  in conductance-based models (1). Indeed, fixed points  $V_*$  of model (4) satisfy

$$f(V_*) = I$$

so that the shape of  $f$  determines the neuro-computational features of the non-spiking model: a monotonic shape involves a near-linear behavior of the model, while an N-shape implies a bistable one with the occurrence of two saddle-node bifurcations. Therefore, the model proposes a simple cubic expression (5) that plays the same role as the complex steady-state

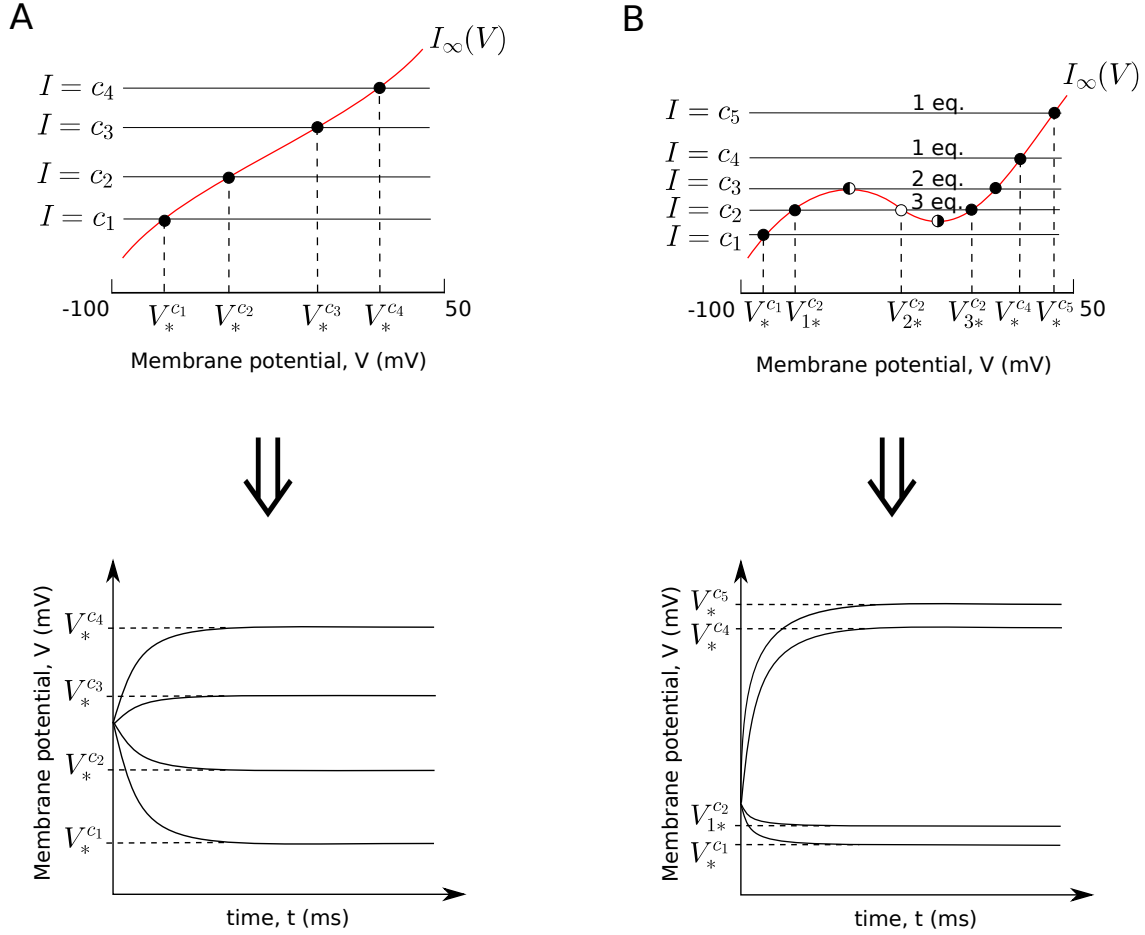


Figure 2: Two typical shapes of the steady-state current  $V \rightarrow I_\infty(V)$ , in red. Intersections of  $I_\infty$  and horizontal line  $I = c$  (with  $c$  constant) correspond to equilibria of the system. We denote stable equilibria as filled circles ●, unstable equilibria as open circles ○ and saddle-node equilibria as ◐. **(A)** (Top) Monotonic steady-state current.  $V_*^{c_i}$ ,  $i = 1, \dots, 4$ , correspond to equilibria for a current injection  $I = c_i$ , respectively. (Bottom) The resulting near-linear voltage dynamics with the four equilibria  $V_*^{c_i}$  showed in (Top). **(B)** (Top) N-shaped steady-state current. The number of equilibria of the system depends on the value of  $I$ . (Bottom) The resulting bistable voltage dynamics with four equilibria  $V_*^{c_i}$  showed in (Top).

current expression (2) of conductance-based models. Parameters  $a$ ,  $b$ ,  $c$  and  $d$  are dimensionless and are estimated in order to fit the experimental steady-state current. Parameter  $\tau$  describes the *constant* time for which  $V$  reaches its equilibrium value  $V_*$ . This parameter

can be either hand-tuned or estimated from experimental voltage.

**Parameter estimation.** Parameters  $a$ ,  $b$ ,  $c$  and  $d$  have been estimated from the 16 points of the steady-state current using differential evolution algorithm (DE) (Storn & Price, 1997). DE is an effective method in the case of parameter estimation of neuronal models (Buhry et al., 2011; Buhry et al., 2012; Naudin et al., 2020), and superior to other optimization methods such as *genetic algorithms*, *simulated annealing* and *particle swarm optimization* in terms of convergence speed, simulation time, and minimization of the cost function (Buhry et al., 2011; Buhry et al., 2008). Moreover, the root-mean-square error normalized to standard deviation (STD) is used as estimator of the model quality (Naudin et al., 2022). Finally, parameter  $\tau$  is set to the value determined in Naudin et al. (2020) and Naudin et al. (2022), estimated to fit experimental voltage traces; however, it can be directly hand-tuned.

**Experimental variability.** For a single target neuron, repetitions of the same external stimulation result in variable electrical responses (Marder & Taylor, 2011) due to multiple sources of intrinsic and extrinsic noise (Destexhe & Rudolph-Lilith, 2012; Faisal et al., 2008). This is why numerous works (Druckmann et al., 2007; Gouwens et al., 2018; Markram et al., 2015) capture the experimental distribution of spiking neuron responses as a more accurate means to describe the neuronal behavior than perfectly replicate a single given experimental voltage trace. This approach seems to be even more suited to non-spiking neurons, which are known to be more sensitive to noise than spiking neurons (Sarpeshkar, 1998). As the steady-state current determines the bifurcation structure of non-spiking neurons and the equilibrium values of their graded responses to particular stimuli, parameters  $a$ ,  $b$ ,  $c$  and  $d$  of the function  $f$  defined in equation (5) are estimated to fit the *mean* of the experimental steady-state current (Figure 1). In this way, the proposed model captures the trial-to-trial variability of a single non-spiking neuron.

**Fundamental differences from simple spiking neuron models and its non-spiking variants.** The steady-state current forms the backbone of the dynamics of non-spiking neurons by determining: (i) all bifurcations of the resting state and the values at which they occur, and (ii) the equilibrium values of their graded responses to particular stimuli. This is not the case for the spiking neurons for which the steady-state current provides only information about *possible* bifurcations of the resting state. Indeed, when the equilibrium loses stability, characteristic of Andronov–Hopf bifurcations responsible for spikes, cannot be inferred from the steady-state current (Izhikevich, 2007). This is why the existing classic simple spiking models were not derived directly from the steady-state current. This explains why these models are inadequate to produce acceptable non-spiking dynamics. Thus, the building of the proposed non-spiking model differs fundamentally from that of existing simple spiking models.

### 3 Results

This section presents the results of the optimization procedure for the three neurons under study and shows how, despite the simplicity of the model, it is able to reproduce bistable and near-linear behaviors with high accuracy. Then, we compare the computational efficiency of the proposed model with respect to conductance-based models developed in Naudin et al. (2020) for the same RIM, AIY and AFD neurons, and many additional types of neuron models. Finally, we implement a canonical example of a non-spiking network of two coupled neurons to demonstrate the ability of the proposed model to explain ‘high-level’ phenomena occurring in non-spiking nervous tissues.

#### 3.1 Results of the optimization procedure

In order to fit the mean of the experimental steady-state current of RIM, AIY and AFD (Figure 1), parameters  $a$ ,  $b$ ,  $c$  and  $d$  of equation (5) are estimated using DE. The parameter

values  $\tau$  are obtained from Naudin et al. (2020) and Naudin et al. (2022) in which they are determined to fit experimental voltage traces. The parameter values are shown in Table 1.

<b>Neuron</b> \ <b>Parameters</b>	$a$	$b$	$c$	$d$	$\tau$ ( $10^{-1}$ s)
<b>RIM</b>	0.000024	0.0036	0.31	7.22	0.042
<b>AIY</b>	0.000044	0.0093	0.773	20.38	0.04
<b>AFD</b>	0.00033	0.048	2.31	38.99	0.06

Table 1: Parameter values of the model (4) for the different neurons. Results for the parameters  $a$ ,  $b$ ,  $c$  and  $d$  are obtained using differential evolution. The parameter  $\tau$  is expressed in ds ( $10^{-1}$  s) and is obtained from Naudin et al. (2020), Naudin et al. (2022).

**Bistable behavior – AFD.** Figure 3 shows the dynamics of the proposed model for the AFD neuron. A high fitting quality of the N-shaped experimental steady-state current mean is obtained (Figure 3.A). Moreover, Figure 3.B shows that the proposed model displays an underlying bifurcation structure specific to non-spiking bistable neurons (Izhikevich, 2007; Naudin et al., 2021; Naudin et al., 2022), with the occurrence of two saddle-node bifurcations. In particular, the voltage jump occurs at  $I \approx 3.1$  pA, exactly as in the CBM relative to AFD neuron published in Naudin et al. (2022). Therefore, the model reproduces the essential features of the AFD neuron, making it adequate for the description of its bistable behavior. Finally, Figure 3.C compares one example of experimental responses of the AFD neuron with the respective dynamics of the model representing the mean of the AFD neuron responses. The large sustained currents of the model (Figure S2), similar to the experimental ones, restrict its membrane potential to two voltages around  $-80$  mV and  $-15$  mV as the experimental neuron behavior. Although the model slightly diverges from the experimental voltage traces, it preserves the main qualitative features of the AFD neuron dynamics.

**Near-linear behavior – RIM and AIY.** Figure 4 shows the dynamics of the proposed model for the RIM and AIY neurons. As in the case of AFD, Figure 4.A (left) illustrates that the model for both neurons fits well with the experimental mean of the steady-state

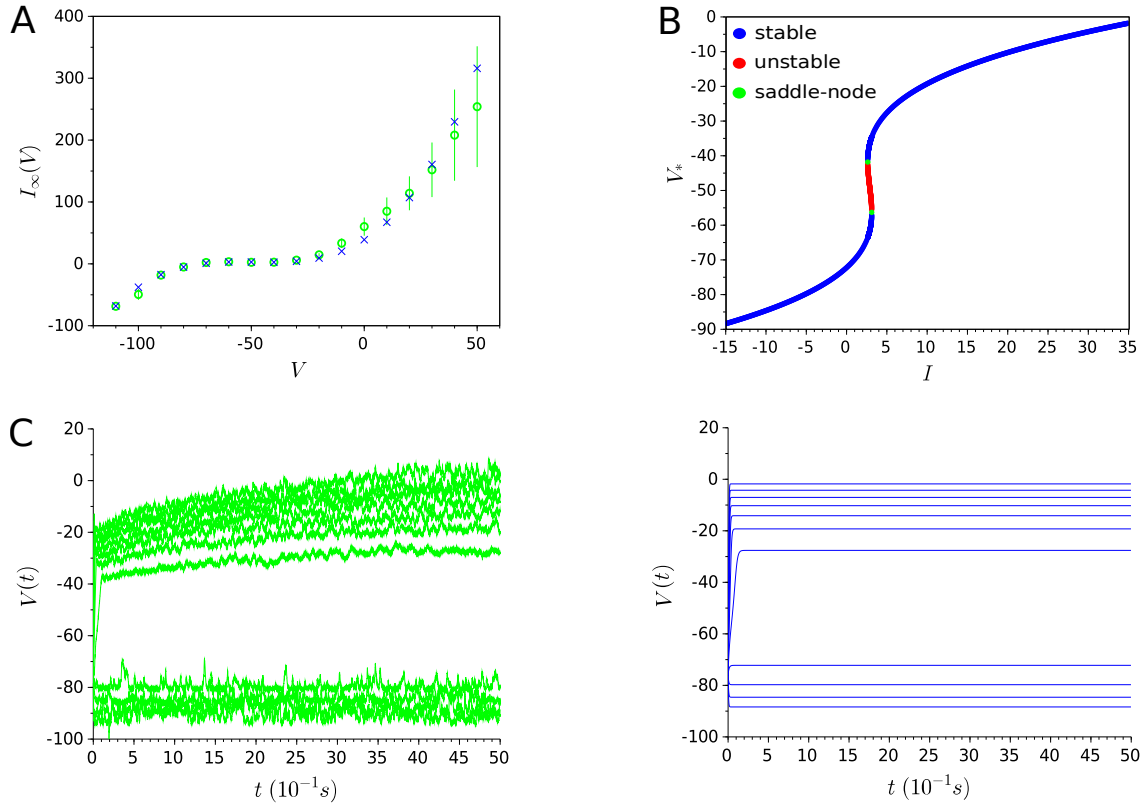


Figure 3: Optimization results for the AFD bistable neuron. **(A)** Mean of the experimental steady-state current (represented by green circles) with respective error bars, and the estimated steady-state current (represented by blue crosses) given by the equation (5) with parameter values displayed in Table 1. **(B)** Bifurcation diagram. The bifurcation structure is typical of bistable non-spiking neurons (Naudin et al., 2021) with the occurrence of two saddle-node bifurcations (at  $I \approx 2.625$  pA and  $I \approx 3.124$  pA). **(C)** Example of experimental responses in AFD (represented in green), and the respective dynamics of the proposed model (represented in blue) representing the variability of the AFD neuron responses. The series of current injections start at  $-15$  pA and increase to  $35$  pA by increments of  $5$  pA.

current. In particular, the monotonic shape of the steady-state current is well captured by the model. The resulting function  $I \mapsto V_*(I)$  is monotonic increasing (Figure 4.A, right), which is typical of non-spiking neurons with a near-linear behavior (Naudin et al., 2021; Naudin et al., 2022). More specifically, the model displays a unique equilibrium point  $V_*$ , that is stable and increases as  $I$  does (Figure 4.A, right), which is consistent with the near-linear behavior

of the experimental data. Finally, Figure 4.B compares one example of the RIM and AIY experimental neuron responses with the dynamics of their respective models representing the mean of their neuronal responses. We can observe that the membrane potential of the AIY model is more sensitive to hyperpolarization than depolarization inputs with a transition point around  $-30$  mV, which is in agreement with the experimental membrane potential behavior of AIY. Moreover, although the simple RIM model does not capture the transient peak in the outward current during voltage clamp (Figure S2), it exhibits a lack of large sustained currents similar to the experimental ones. This allows it to be depolarized or hyperpolarized in a smooth manner under current clamp, as its experimental voltage dynamics.

### 3.2 Computational efficiency.

**Model simulation.** To evaluate the computational efficiency of the model simulation, we compare the number of floating point operations (FLOPs), such as addition, multiplication or division, required to simulate 1ms (FLOPMS) of different neuron models. Note that the values of FLOPMS are related to the simulation time and not to the running time, which may vary widely across programming languages and CPU architectures. The simulation of the proposed model only takes 13 floating point operations to simulate the span of 1 ms in the neuron. These results are of the same order of magnitude as the integrate-and-fire and Izhikevich models that are the most computational efficient neuron models to date (Izhikevich, 2004). In order to establish comparisons, the CBMs relative to RIM, AIY and AFD neurons (see Appendix A) published in Naudin et al. (2020) have a computational efficiency similar to the Hodgkin–Huxley model which requires about 1200 FLOPMS (Izhikevich, 2004). That shows the large superiority of the proposed model when compared to the CBMs proposed in Naudin et al. (2020) in terms of computational efficiency.

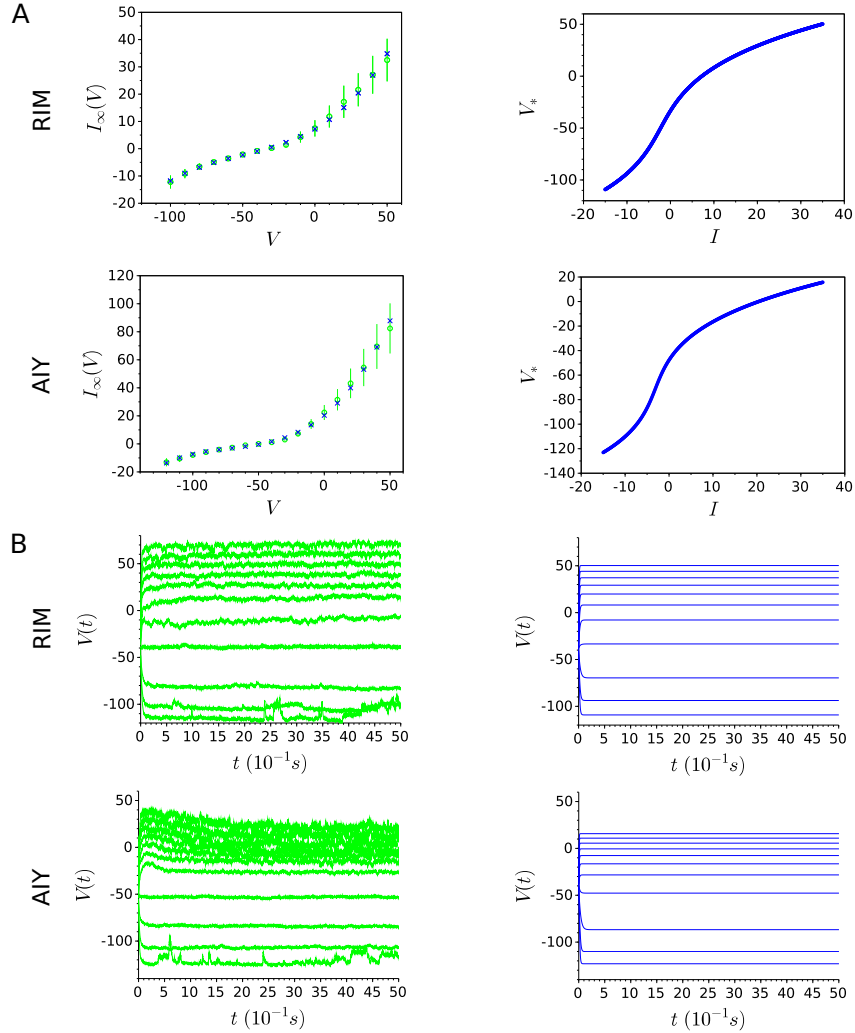


Figure 4: Optimization results for the RIM and AIY near-linear neurons. **(A)** (Left) Mean of the experimental steady-state current (represented by green circles) with respective error bars, and the estimated steady-state current (represented by blue crosses) given by the equation (5) with parameter values displayed in Table 1. (Right) Function  $I \mapsto V_*(I)$  for all  $I \in [-15 \text{ pA}; 35 \text{ pA}]$ . In both cases, the function is monotonic increasing, meaning that  $V_*$  increases as  $I$  does which is consistent with the experimental behavior displayed in Figure 1. **(B)** (Left) Example of experimental responses in RIM and AIY, represented in green. (Right) Respective dynamics of the proposed model, represented in blue, representing the mean of their neuronal responses. The series of current injections start from  $-15 \text{ pA}$  and increase to  $35 \text{ pA}$  by  $5 \text{ pA}$  increments.



**Model optimization.** As discussed in Section 2, the steady-state current determines the bifurcation structure of non-spiking neurons as well as the equilibrium values of their graded responses. In this way, all parameters of the proposed model are directly estimated from steady-state current data. On the contrary, the same procedure cannot be applied to estimate the parameters of a CBM as the parametrization space is larger and requires voltage trace data (see, *e.g.*, Appendix A). The consequence is that the optimization process of the proposed model is computationally much more efficient than that of a CBM: while a cost-function call in the proposed model requires evaluation of around 16 points (number of points of the steady-state current, see Figure 1), a CBM requires to evaluate, as in Naudin et al. (2020), around 137500 points per function call (11 voltage traces  $\times$  12500 points per trace). In practical terms, this means that estimating all the parameters of a CBM using DE is in the order of some days of computing (Naudin et al., 2020), while estimating all the parameters of the proposed model in this paper took only a few seconds. It is outside the scope of this paper to establish a quantitative computational comparison between the optimization times in both models, as that would require to replicate the experiments in a controlled computational environment. However, we can safely conclude that the optimization process of the proposed model is computationally more efficient than that of a CBM in several orders of magnitude.

**Model building.** Another advantage of the proposed model is that it requires less biophysical information for its conception than a CBM. In particular, a CBM imposes a detailed modeling of the different ion channels present in the cell membrane, for which it is necessary to have contrasted biological data obtained in the laboratory. Such data are often very time-consuming and hard to obtain experimentally, as reported for the *C. elegans* neurons (Goodman et al., 2012) due to their small size and the difficulty of dissecting a one-millimeter-long worm. That is not the case of the proposed model as it relies only on the steady-state current data and not on the biophysical information of the ion channels.

### 3.3 Generalization capability of the proposed model

A good neuronal model should be able to predict the neuronal activity based on data that were not used for parameter tuning (Gerstner & Naud, 2009). Indeed, capturing the neuron behavior for some inputs may not be sufficient to predict acceptable responses to different novel stimuli not used during the models' building (Druckmann, 2014; Druckmann et al., 2011; Naudin et al., 2022). A way to endow a neuron model with generalization capabilities is to reproduce the bifurcation structure of the neuron (Izhikevich, 2007; Naudin et al., 2022). We stated in Section 2 that the steady-state current determines the bifurcation structure of non-spiking neurons and the equilibrium values of their graded responses to particular stimuli. Since the parameters of the proposed model are determined from the fitting of the steady-state current, the model will acquire the generalization capability directly from the optimization process. While this is granted in the proposed model by design, it is usually not the case in CBM where capturing the bifurcation structure is not the primary objective. Figure S3 shows a representative example of the deterioration of the steady-state current of a non-spiking CBM, as well as its dramatic implication on the neuron dynamics and its generalization capability. Naudin et al. (2022) propose in the case of non-spiking neurons to capture it by considering the steady-state current as an additional objective to be reproduced, in addition to fitting the membrane potential evolution. Such a multi-objective approach is successful but takes a very long time (about ten days). Therefore, the optimization and building process of the proposed model are efficient in the sense that it endows the models with generalization capabilities without requiring additional procedures with a high computational cost.

### 3.4 Implementation of a canonical non-spiking neuronal network

This section aims to demonstrate the capability of the proposed model to explain 'high-level' experimental phenomena occurring in non-spiking nervous tissues. To that end, we implement a canonical non-spiking neural network of two coupled neurons through an excitatory synapse. This network represents a bistable sensory neuron (such as AFD) that propagates electrical

signals to a postsynaptic near-linear neuron (such as RIM). The synaptic transmission is considered graded as it is the case in non-spiking nervous tissues, such as in the vertebrate retina (Tsukamoto et al., 2001), the *Ascaris* (Davis & Stretton, 1989) and *C. elegans* (Lindsay et al., 2011) worms. Following Wicks et al. (1996), the mathematical expression of the network is given by

$$\begin{cases} \tau_1 \frac{dV_1}{dt} = -a_1 V_1^3 - b_1 V_1^2 - c_1 V_1 - d_1 + I \\ \tau_2 \frac{dV_2}{dt} = -a_2 V_2^3 - b_2 V_2^2 - c_2 V_2 - d_2 - g_{syn} g_\infty(V_1)(V_2 - 0) \end{cases}$$

where  $V_1$  represents the membrane potential of the presynaptic bistable sensory neuron,  $V_2$  the membrane potential of the postsynaptic near-linear neuron,  $I$  the external sensory input current,  $g_{syn}$  the maximal postsynaptic membrane conductance for the synapse, and  $V \mapsto g_\infty(V)$  a sigmoid function relating presynaptic and postsynaptic membrane potential. Its expression reads as

$$g_\infty(V) = \frac{1}{1 + \exp\left(\frac{V - V_{rest}}{V_{slope}}\right)}$$

with  $V_{rest}$  the presynaptic resting potential, and  $V_{slope}$  is the slope factor of the sigmoid function  $g_\infty$ . In the following, we set  $V_{slope} = 15$  mV,  $g_{syn} = 0.6$  nS and  $V_{rest} = -76$  mV (Wicks et al., 1996).

The purpose is to monitor the dynamics of the RIM neuron when it receives inputs from a bistable neuron. To that end, the AFD sensory neuron is stimulated with a series of current injections starting from  $-15$  pA and increasing to  $35$  pA by  $5$  pA increments. As can be seen in Figure 5, the near-linear RIM neuron (Figure 5.A) becomes bistable under the effect of the coupling with the bistable AFD neuron (Figure 5.B, left). Transitions between down-states and up-states are apparent in the bimodal distribution of the membrane potential (Figure 5.B, right). Thus, it can be concluded that the connectivity of a neuron affects strongly the nature of its behavior: for instance, a near-linear neuron can become bistable when coupled

with another bistable neuron. Among others, this can explain the discrepancy between the near-linear electrophysiological behavior of the RIM neuron (Figure 1.A) and its bistable calcium dynamics when exposed to odor stimuli (Gordus et al., 2015). Furthermore, these results illustrate the importance of the synaptic dynamics in conferring distinct up- and down-states to non-spiking neurons. Whole-brain calcium imaging of neuronal activity in *C. elegans* reveals that several dozens of non-spiking neurons have collective activity with such correlated up- and down-states (Prevedel et al., 2014; Schrödel et al., 2013). The results presented in this paper suggest that the proposed model may be used to gain insights into synaptic dynamics in these network states.

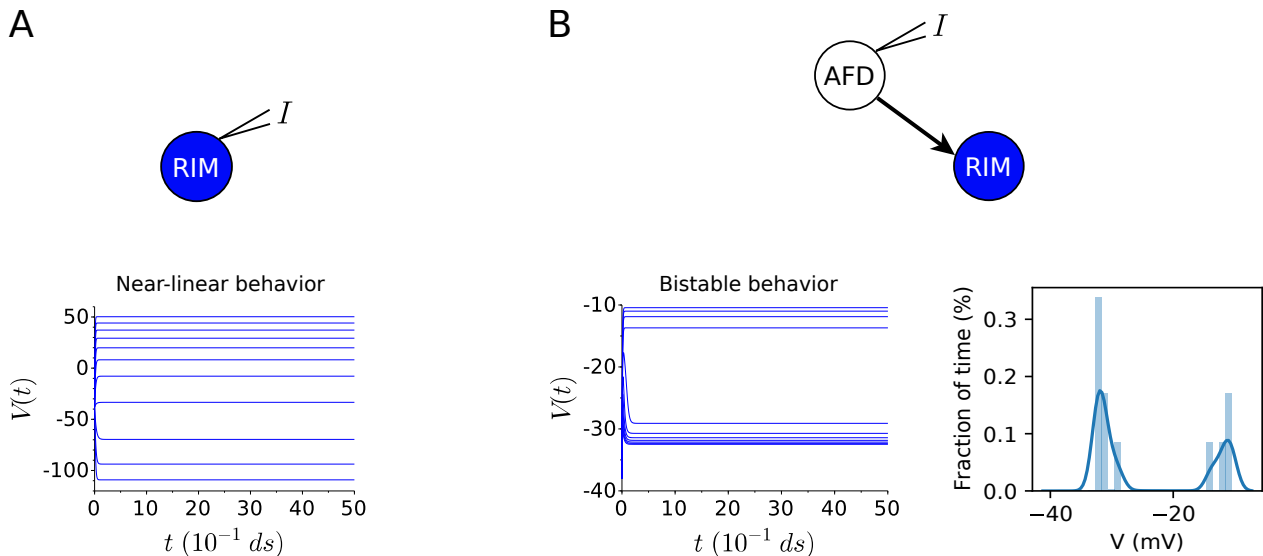


Figure 5: Voltage dynamics of the RIM neuron. **(A)** Evolution of the near-linear membrane potential of the RIM neuron for a series of injection currents  $I$ , from  $-15$  pA to  $35$  pA by  $5$  pA increments. **(B)** (Left) Evolution of voltages of the RIM neuron when its presynaptic AFD bistable neuron is stimulated by current steps, from  $-15$  pA to  $35$  pA by  $5$  pA increments. AFD and RIM are coupled through an excitatory synapse. Synaptic parameters:  $g_{syn} = 0.6$  nS (Wicks et al., 1996) and  $V_{slope} = 15$  mV. (Right) Corresponding histogram of the membrane potential calculated from  $50$  ds ( $5000$  ms) of simulation.

## 4 Discussion

Various computationally efficient and simple spiking models have been proposed in the literature as an alternative to Hodgkin–Huxley type models. Such models have been valuable to gain insight into ‘higher-level’ functions of neural systems. Unfortunately, these simple models have a bifurcation structure that differs fundamentally from that of non-spiking neurons. This makes them inadequate for producing acceptable non-spiking dynamics, which are also ubiquitous in neuronal processes. To the best of our knowledge, this paper is a first attempt to develop a simple model specifically built on the basis of the bifurcation structure of non-spiking neurons. This model was then shown to have a high computational efficiency, to be able to accurately capture the individual experimental qualitative behavior of known types of non-spiking neurons, to generalize neuronal responses, and to explain and reproduce ‘high-level’ experimental phenomena in non-spiking networks. This section aims at discussing both the biological and the modeling implications of such a model from two perspectives: the modeling of the *C. elegans* neuronal network and retinal networks.

**Implications to the modeling of the *C. elegans* neuronal network.** The *C. elegans* nervous system is only composed of 302 neurons and about 7000 synaptic connections, and its connectome has been fully mapped (White et al., 1986). Despite this relative simplicity, the nematode shares many features with the complex human nervous system using similar neurotransmitters, ion channels and developmental genes, as well as similar neuronal principles to produce behavior (Chalasan et al., 2007; P. Liu et al., 2020). For these reasons, it has become the ideal candidate to be modeled to investigate how behavior emerges from underlying physiological processes (Costalago-Meruelo et al., 2018; Izquierdo, 2019; Lanza et al., 2021; Olivares et al., 2019; Szigeti et al., 2014). However, as pointed out by Sarma et al. (2018), such modeling studies do not take into account the specificity of *C. elegans* neuronal dynamics. Building models adapted to the nematode neuron dynamics is a key remaining component to make *C. elegans* nervous system modeling adequate for biological research

(Sarma et al., 2018). The simple and computationally efficient model proposed in this paper, capable of reproducing the known neuronal diversity of *C. elegans* neurons, could serve as a building block to study ‘higher-level’ functions of the *C. elegans* neuronal activity, such as determining the nature (excitatory or inhibitory) and strength of its synaptic connections. Indeed, such information is not revealed by the connectome (Kopell et al., 2014) and is of crucial importance to understand the flow of information within the nematode’s nervous system (Bargmann & Marder, 2013). Some computational works (Costalago-Meruelo et al., 2018; Lanza et al., 2021; Olivares et al., 2019; Portegys, 2015; Wicks et al., 1996) estimate the synaptic polarity using an evolutionary approach in which the algorithm determines both the nature and the strength of connections to obtain observable, realistic worm behavior. However, the networks studied are composed of neuron models that are not representative of the *C. elegans* neuron dynamics. For instance, Portegys (2015), Costalago-Meruelo et al. (2018) and Lanza et al. (2021) consider a homogeneous spiking model for the entire network although the *C. elegans* neurons are highly heterogeneous and contain non-spiking neurons (Goodman et al., 1998). Therefore, even if the macroscopic behavior of *C. elegans* is successfully reproduced, the results on the synaptic polarity and their strength may not be biologically adequate. We suggest that the proposed model could provide a simple and efficient way to build models adapted to the *C. elegans* neuronal dynamics in order to make *C. elegans* modeling studies adequate for biological research.

**Implications to the modeling of the retinal network.** Due to the common origins of the retina and the brain, it is suggested that the neuronal activity in the retina and the brain correlates, so that changes in the retina may indicate structural and functional changes in the brain. Many authors then consider “the retina as a window to the brain” (London et al., 2013). This is why the modeling of the retinal network could be a valuable tool to investigate various neuronal phenomena. Interestingly, the neuronal characteristics of the retina are similar to those of *C. elegans* in several aspects. First, the worm olfactory system and the retinal visual system of vertebrates follow the same general principles to

process sensory information (Chalasanani et al., 2007). Second, the retina neurons release neurotransmitter in a graded and tonic manner (Tsukamoto et al., 2001; Werblin & Dowling, 1969) as the *C. elegans* (Lindsay et al., 2011). Third, non-spiking neurons are also ubiquitous in the retina.

The retinal circuit is composed of several major classes of neurons: rod and cone photoreceptors, and horizontal, bipolar, amacrine and retinal ganglion cells (RCGs). Only RCGs and some amacrine cells trigger action potentials, while the other cells transmit visual information using graded potentials. More specifically, the cone (Kourennyi et al., 2004), horizontal (Aoyama et al., 2000) and bipolar cells (Schilardi & Kleinlogel, 2021; Usui et al., 1996) exhibit a bistable behavior (such as the *C. elegans* AFD neuron considered in this paper), while the rod (Kourennyi et al., 2004) and amacrine cells display a near-linear one (such as RIM and AIY). These neurons number in the tens of millions (Field & Chichilnisky, 2007). Moreover, each major retinal cell class consists of multiple cell types distinguished by variable response properties (Field & Chichilnisky, 2007). From a general point of view, this neuron-to-neuron variability has been shown to play a paramount role in network performance (Berry Ii et al., 2019; Lengler et al., 2013; Padmanabhan & Urban, 2010; Shamir & Sompolinsky, 2006). This demonstrates the importance of generating many models to capture every individual neuron behavior within the biological population, rather than using a unique model for the entire population (Marder & Taylor, 2011). Based on the fitting of the steady-state current that takes only a few seconds, the proposed model makes possible the generation of multiple models to capture the substantial neuron-to-neuron variability of retinal cells.

## Acknowledgements

This work was supported by the ERDF (XTerm Project), Normandie Region (France) and by The LMAH, FR-CNRS-3335.

## Code Accessibility

The code of differential evolution algorithm for parameter estimation is available at <https://github.com/lois76/codeDEnewGPmodel>. Raw electrophysiological recording traces are available into Mendeley at <https://doi.org/10.17632/tngf9w3pgd.1>

## Declaration of Competing Interests

The authors declare no competing interests.



## A Appendix: Conductance-based models of the RIM, AIY and AFD neurons

In previous works (Naudin et al., 2020; Naudin et al., 2022), we determined the most suitable conductance-based models to the electrophysiology of the RIM, AIY and AFD neurons based on current biological research and a series of in-silico experiments.

**Neuron models.** For the RIM and AFD neurons, the  $I_{Ca,p} + I_{Kir} + I_{K,t} + I_L$ -model was obtained which reads as

$$\left\{ \begin{array}{l} C\dot{V} = -g_{Ca}m_{Ca}(V - E_{Ca}) - g_{Kir}h_{Kir\infty}(V)(V - E_K) - g_Km_Kh_K(V - E_K) \\ \quad -g_L(V - E_L) + I \\ \dot{m}_{Ca} = \frac{m_{Ca\infty}(V) - m_{Ca}}{\tau_{m_{Ca}}}, \quad m_{Ca\infty}(V) = \left(1 + \exp\left(\frac{V_{1/2}^{m_{Ca}} - V}{k_{m_{Ca}}}\right)\right)^{-1} \\ \dot{m}_K = \frac{m_{K\infty}(V) - m_K}{\tau_{m_K}}, \quad m_{K\infty}(V) = \left(1 + \exp\left(\frac{V_{1/2}^{m_K} - V}{k_{m_K}}\right)\right)^{-1} \\ \dot{h}_K = \frac{h_{K\infty}(V) - h_K}{\tau_{h_K}}, \quad h_{K\infty}(V) = \left(1 + \exp\left(\frac{V_{1/2}^{h_K} - V}{k_{h_K}}\right)\right)^{-1} \end{array} \right. \quad (6)$$

whereas for the AIY neuron, the  $I_{Ca,t} + I_{Kir} + I_{K,p} + I_L$ -model was selected taking the form

$$\left\{ \begin{array}{l} C\dot{V} = -g_{Ca}m_{Ca}h_{Ca}(V - E_{Ca}) - g_{Kir}h_{Kir\infty}(V)(V - E_K) - g_Km_K(V - E_K) \\ \quad -g_L(V - E_L) + I \\ \dot{m}_{Ca} = \frac{m_{Ca\infty}(V) - m_{Ca}}{\tau_{m_{Ca}}}, \quad m_{Ca\infty}(V) = \left(1 + \exp\left(\frac{V_{1/2}^{m_{Ca}} - V}{k_{m_{Ca}}}\right)\right)^{-1} \\ \dot{h}_{Ca} = \frac{h_{Ca\infty}(V) - h_{Ca}}{\tau_{h_{Ca}}}, \quad h_{Ca\infty}(V) = \left(1 + \exp\left(\frac{V_{1/2}^{h_{Ca}} - V}{k_{h_{Ca}}}\right)\right)^{-1} \\ \dot{m}_K = \frac{m_{K\infty}(V) - m_K}{\tau_{m_K}}, \quad m_{K\infty}(V) = \left(1 + \exp\left(\frac{V_{1/2}^{m_K} - V}{k_{m_K}}\right)\right)^{-1} \end{array} \right. \quad (7)$$

**Expression of the steady-state currents.** The steady-state current relative to the system of equations (6) takes the form

$$I_{\infty}(V_H) = g_{Ca}m_{Ca\infty}(V_H)(V_H - E_{Ca}) + g_{Kir}h_{Kir\infty}(V_H)(V_H - E_K) \\ + g_Km_{K\infty}(V_H)h_{K\infty}(V_H)(V_H - E_K) + g_L(V_H - E_L)$$

whereas for the system of equations (7), it is defined as

$$I_{\infty}(V_H) = g_{Ca}m_{Ca\infty}(V_H)h_{Ca\infty}(V_H)(V_H - E_{Ca}) + g_{Kir}h_{Kir\infty}(V_H)(V_H - E_K) \\ + g_Km_{K\infty}(V_H)(V_H - E_K) + g_L(V_H - E_L)$$

## B Appendix: Supplementary figures

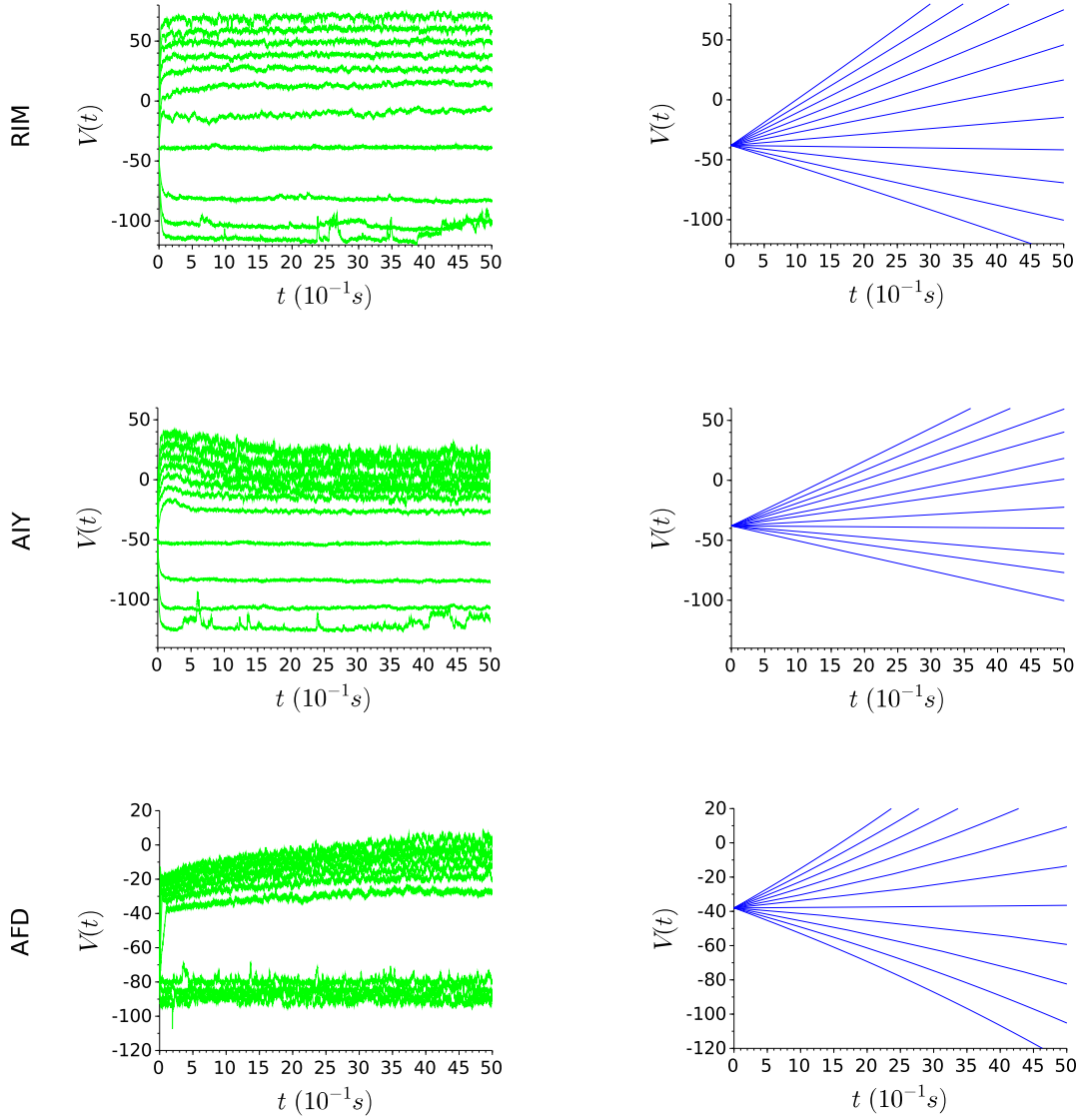


Figure S1: (Left) Examples of experimental membrane potentials of RIM, AIY and AFD neurons induced by a series of current steps starting from  $-15$  pA and increasing to  $35$  pA in  $5$  pA increments (Q. Liu et al., 2018). (Right) Membrane potentials of the best solution of the leaky integrate-and-fire model designed with a threshold high enough to avoid the triggering of spikes, as in Strohmer et al. (2021). The solutions are obtained from the fitting of experimental voltage traces in (Left) using differential evolution algorithm. The series of current injections is the same than in (Left).

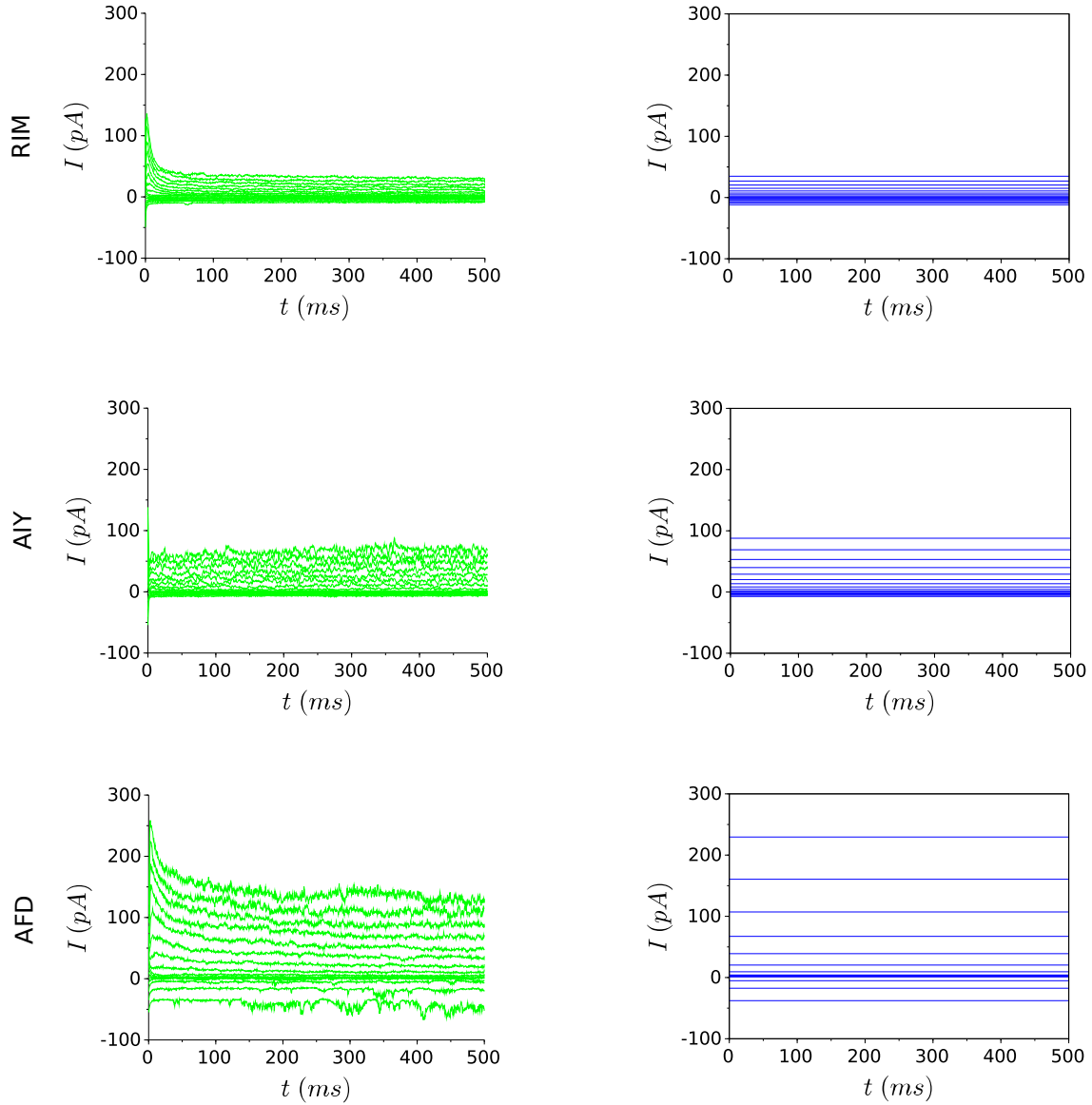


Figure S2: (Left) Examples of experimental whole-cell current traces of RIM, AIY and AFD neurons induced by a series of voltage steps starting from  $-100$  mV and increasing to  $50$  mV in  $10$  mV increments (Q. Liu et al., 2018). (Right) Whole-cell current traces of the simple proposed model induced by the same voltage step protocol.

## References

- Aoyama, T., Kamiyama, Y., Usui, S., Blanco, R., Vaquero, C. F., & de la Villa, P. (2000). Ionic current model of rabbit retinal horizontal cell. *Neuroscience Research*, *37*(2), 141–151.

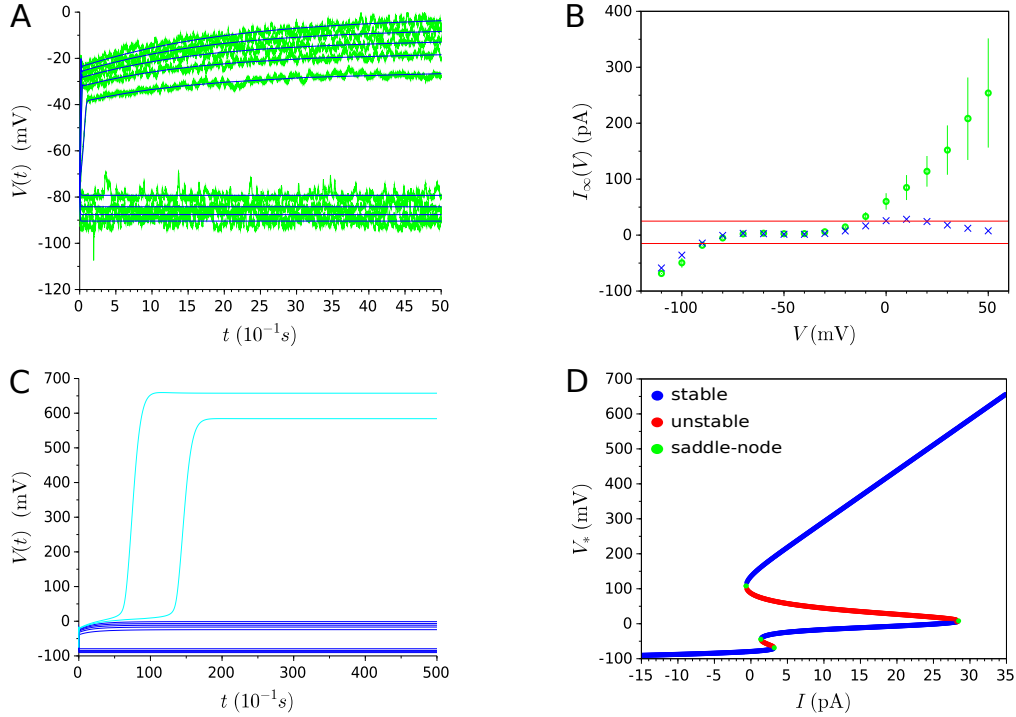


Figure S3: Example of dramatic implications of the deterioration of the steady-state current on the neuron dynamics and its generalization ability. **(A)** Experimental data (represented in green) and  $I_{Ca,p} + I_{Kir} + I_{K,t} + I_L$ -model (represented in blue) overlap for a series of current injections starting from  $-15 \text{ pA}$  and increasing to  $25 \text{ pA}$  by  $5 \text{ pA}$  increments. **(B)** Experimental steady-state currents (represented by green circles) and estimated steady-state currents (represented by blue crosses) resulting from the fitting of membrane potential evolution in (A). Red lines delineate the interval  $[-15 \text{ pA}, 25 \text{ pA}]$ . In this interval, the experimental steady-state current is accurately reproduced, but the model completely deteriorates for values higher than  $25 \text{ pA}$ . **(C)** Dark blue curves represent the evolution of membrane potential for the same values of current injection than in (A) (*i.e.* stimuli starting from  $-15 \text{ pA}$  and increasing to  $25 \text{ pA}$  by  $5 \text{ pA}$  increments), whereas light blue ones represent the drastic non-physiological change of voltage traces for novel stimuli ( $30 \text{ pA}$  and  $35 \text{ pA}$ ). Note the difference of scale regarding y-axis between (A) and (C). **(D)** Bifurcation diagram. Four saddle-node bifurcations occur at  $I \approx -0.66 \text{ pA}$ ,  $I \approx 1.36 \text{ pA}$ ,  $I \approx 3.19 \text{ pA}$  and  $I \approx 28.4 \text{ pA}$ . This figure has been extracted from Naudin et al. (2022) with the consent of the authors.

- Aussel, A., Buhry, L., Tyvaert, L., & Ranta, R. (2018). A detailed anatomical and mathematical model of the hippocampal formation for the generation of sharp-wave ripples and theta-nested gamma oscillations. *Journal of computational neuroscience*, *45*(3), 207–221.
- Bargmann, C. I., & Marder, E. (2013). From the connectome to brain function. *Nature methods*, *10*(6), 483.
- Berry II, M. J., Lebois, F., Ziskind, A., & da Silveira, R. A. (2019). Functional diversity in the retina improves the population code. *Neural computation*, *31*(2), 270–311.
- Brenner, S. (1974). The genetics of *caenorhabditis elegans*. *Genetics*, *77*(1), 71–94.
- Buhry, L., Grassia, F., Giremus, A., Grivel, E., Renaud, S., & Saïghi, S. (2011). Automated parameter estimation of the hodgkin-huxley model using the differential evolution algorithm: Application to neuromimetic analog integrated circuits. *Neural computation*, *23*(10), 2599–2625.
- Buhry, L., Pace, M., & Saïghi, S. (2012). Global parameter estimation of an hodgkin–huxley formalism using membrane voltage recordings: Application to neuro-mimetic analog integrated circuits. *Neurocomputing*, *81*, 75–85.
- Buhry, L., Saïghi, S., Giremus, A., Grivel, E., & Renaud, S. (2008). Parameter estimation of the hodgkin-huxley model using metaheuristics: Application to neuromimetic analog integrated circuits. *2008 IEEE Biomedical Circuits and Systems Conference*, 173–176.
- Burrows, M., Laurent, G., & Field, L. (1988). Proprioceptive inputs to nonspiking local interneurons contribute to local reflexes of a locust hindleg. *Journal of Neuroscience*, *8*(8), 3085–3093.
- Chalasan, S. H., Chronis, N., Tsunozaki, M., Gray, J. M., Ramot, D., Goodman, M. B., & Bargmann, C. I. (2007). Dissecting a circuit for olfactory behaviour in *caenorhabditis elegans*. *Nature*, *450*(7166), 63.

- Costalago-Meruelo, A., Machado, P., Appiah, K., Mujika, A., Leskovsky, P., Alvarez, R., Epelde, G., & McGinnity, T. M. (2018). Emulation of chemical stimulus triggered head movement in the *c. elegans* nematode. *Neurocomputing*, *290*, 60–73.
- Davis, R. E., & Stretton, A. (1989). Signaling properties of ascaris motorneurons: Graded active responses, graded synaptic transmission, and tonic transmitter release. *Journal of Neuroscience*, *9*(2), 415–425.
- Destexhe, A., & Rudolph-Lilith, M. (2012). *Neuronal noise* (Vol. 8). Springer Science & Business Media.
- Druckmann, S. (2014). Automated parameter constraining of single-neuron models. *The computing dendrite* (pp. 465–482). Springer.
- Druckmann, S., Banitt, Y., Gidon, A. A., Schürmann, F., Markram, H., & Segev, I. (2007). A novel multiple objective optimization framework for constraining conductance-based neuron models by experimental data. *Frontiers in neuroscience*, *1*, 1.
- Druckmann, S., Berger, T. K., Schürmann, F., Hill, S., Markram, H., & Segev, I. (2011). Effective stimuli for constructing reliable neuron models. *PLoS Comput Biol*, *7*(8), e1002133.
- Faisal, A. A., Selen, L. P., & Wolpert, D. M. (2008). Noise in the nervous system. *Nature reviews neuroscience*, *9*(4), 292–303.
- Field, G. D., & Chichilnisky, E. (2007). Information processing in the primate retina: Circuitry and coding. *Annu. Rev. Neurosci.*, *30*, 1–30.
- FitzHugh, R. (1961). Impulses and physiological states in theoretical models of nerve membrane. *Biophysical journal*, *1*(6), 445–466.
- Gerstner, W., & Naud, R. (2009). How good are neuron models? *Science*, *326*(5951), 379–380.
- Giovannini, F., Knauer, B., Yoshida, M., & Buhry, L. (2017). The can-in network: A biologically inspired model for self-sustained theta oscillations and memory maintenance in the hippocampus. *Hippocampus*, *27*(4), 450–463.

- Goodman, M. B., Hall, D. H., Avery, L., & Lockery, S. R. (1998). Active currents regulate sensitivity and dynamic range in *c. elegans* neurons. *Neuron*, *20*(4), 763–772.
- Goodman, M. B., Lindsay, T. H., Lockery, S. R., & Richmond, J. E. (2012). Electrophysiological methods for *caenorhabditis elegans* neurobiology. *Methods in cell biology*, *107*, 409–436.
- Gordus, A., Pokala, N., Levy, S., Flavell, S. W., & Bargmann, C. I. (2015). Feedback from network states generates variability in a probabilistic olfactory circuit. *Cell*, *161*(2), 215–227.
- Górski, T., Depannemaecker, D., & Destexhe, A. (2021). Conductance-based adaptive exponential integrate-and-fire model. *Neural Computation*, *33*(1), 41–66.
- Gouwens, N. W., Berg, J., Feng, D., Sorensen, S. A., Zeng, H., Hawrylycz, M. J., Koch, C., & Arkhipov, A. (2018). Systematic generation of biophysically detailed models for diverse cortical neuron types. *Nature communications*, *9*(1), 1–13.
- Hodgkin, A. L., & Huxley, A. F. (1952). A quantitative description of membrane current and its application to conduction and excitation in nerve. *The Journal of physiology*, *117*(4), 500–544.
- Izhikevich, E. M. (2001). Resonate-and-fire neurons. *Neural networks*, *14*(6-7), 883–894.
- Izhikevich, E. M. (2003). Simple model of spiking neurons. *IEEE Transactions on neural networks*, *14*(6), 1569–1572.
- Izhikevich, E. M. (2004). Which model to use for cortical spiking neurons? *IEEE transactions on neural networks*, *15*(5), 1063–1070.
- Izhikevich, E. M. (2007). *Dynamical systems in neuroscience*. MIT press.
- Izquierdo, E. J. (2019). Role of simulation models in understanding the generation of behavior in *c. elegans*. *Current Opinion in Systems Biology*, *13*, 93–101.
- Kamiyama, Y., Wu, S. M., & Usui, S. (2009). Simulation analysis of bandpass filtering properties of a rod photoreceptor network. *Vision research*, *49*(9), 970–978.



- Kopell, N. J., Gritton, H. J., Whittington, M. A., & Kramer, M. A. (2014). Beyond the connectome: The dynamo. *Neuron*, *83*(6), 1319–1328.
- Kourennyi, D. E., Liu, X.-d., Hart, J., Mahmud, F., Baldrige, W. H., & Barnes, S. (2004). Reciprocal modulation of calcium dynamics at rod and cone photoreceptor synapses by nitric oxide. *Journal of neurophysiology*, *92*(1), 477–483.
- Kuramochi, M., & Doi, M. (2017). A computational model based on multi-regional calcium imaging represents the spatio-temporal dynamics in a caenorhabditis elegans sensory neuron. *PLoS One*, *12*(1), e0168415.
- Lanza, E., Di Angelantonio, S., Gosti, G., Ruocco, G., & Folli, V. (2021). A recurrent neural network model of c. elegans responses to aversive stimuli. *Neurocomputing*, *430*, 1–13.
- Latham, P. E., Richmond, B., Nelson, P., & Nirenberg, S. (2000). Intrinsic dynamics in neuronal networks. i. theory. *Journal of neurophysiology*, *83*(2), 808–827.
- Laurent, G., & Burrows, M. (1989a). Intersegmental interneurons can control the gain of reflexes in adjacent segments of the locust by their action on nonspiking local interneurons. *Journal of Neuroscience*, *9*(9), 3030–3039.
- Laurent, G., & Burrows, M. (1989b). Distribution of intersegmental inputs to nonspiking local interneurons and motor neurons in the locust. *Journal of Neuroscience*, *9*(9), 3019–3029.
- Lengler, J., Jug, F., & Steger, A. (2013). Reliable neuronal systems: The importance of heterogeneity. *PloS one*, *8*(12), e80694.
- Lindsay, T. H., Thiele, T. R., & Lockery, S. R. (2011). Optogenetic analysis of synaptic transmission in the central nervous system of the nematode caenorhabditis elegans. *Nature communications*, *2*(1), 1–9.
- Liu, P., Chen, B., & Wang, Z.-W. (2020). Gabaergic motor neurons bias locomotor decision-making in c. elegans. *Nature Communications*, *11*(1), 1–19.
- Liu, Q., Kidd, P. B., Dobosiewicz, M., & Bargmann, C. I. (2018). C. elegans awa olfactory neurons fire calcium-mediated all-or-none action potentials. *Cell*, *175*(1), 57–70.

- Lockery, S. R., Goodman, M. B., & Faumont, S. (2009). First report of action potentials in a *c. elegans* neuron is premature. *Nature neuroscience*, *12*(4), 365–366.
- London, A., Benhar, I., & Schwartz, M. (2013). The retina as a window to the brain—from eye research to cns disorders. *Nature Reviews Neurology*, *9*, 44–53.
- Marder, E., & Taylor, A. L. (2011). Multiple models to capture the variability in biological neurons and networks. *Nature neuroscience*, *14*(2), 133–138.
- Marín, M., Sáez-Lara, M. J., Ros, E., & Garrido, J. A. (2020). Optimization of efficient neuron models with realistic firing dynamics. the case of the cerebellar granule cell. *Frontiers in Cellular Neuroscience*, *14*, 161.
- Markram, H., Muller, E., Ramaswamy, S., Reimann, M. W., Abdellah, M., Sanchez, C. A., Ailamaki, A., Alonso-Nanclares, L., Antille, N., Arsever, S., et al. (2015). Reconstruction and simulation of neocortical microcircuitry. *Cell*, *163*(2), 456–492.
- Naudin, L., Corson, N., & Alaoui, M. A. (2021). A generic conductance-based model of non-spiking *caenorhabditis elegans* neurons and its mathematical analysis.
- Naudin, L., Corson, N., Aziz-Alaoui, M., Laredo, J. L. J., & Démare, T. (2020). On the modeling of the three types of non-spiking neurons of the *caenorhabditis elegans*. *International Journal of Neural Systems*, S012906572050063X.
- Naudin, L., Jiménez Laredo, J. L., Liu, Q., & Corson, N. (2022). Systematic generation of biophysically detailed models with generalization capability for non-spiking neurons. *PloS one*, *17*(5), e0268380.
- Nicoletti, M., Loppini, A., Chiodo, L., Folli, V., Ruocco, G., & Filippi, S. (2019). Biophysical modeling of *c. elegans* neurons: Single ion currents and whole-cell dynamics of *awcon* and *rmd*. *PloS one*, *14*(7), e0218738.
- O’Leary, T., Sutton, A. C., & Marder, E. (2015). Computational models in the age of large datasets. *Current opinion in neurobiology*, *32*, 87–94.
- Olivares, E., Izquierdo, E., & Beer, R. (2019). A neuromechanical model of multiple network oscillators for forward locomotion in *c. elegans*. *BioRxiv*, 710566.

- Padmanabhan, K., & Urban, N. N. (2010). Intrinsic biophysical diversity decorrelates neuronal firing while increasing information content. *Nature neuroscience*, *13*(10), 1276–1282.
- Poirazi, P., & Papoutsis, A. (2020). Illuminating dendritic function with computational models. *Nature Reviews Neuroscience*, 1–19.
- Portegys, T. E. (2015). Training sensory–motor behavior in the connectome of an artificial *c. elegans*. *Neurocomputing*, *168*, 128–134.
- Prevedel, R., Yoon, Y.-G., Hoffmann, M., Pak, N., Wetzstein, G., Kato, S., Schrödel, T., Raskar, R., Zimmer, M., Boyden, E. S., et al. (2014). Simultaneous whole-animal 3d imaging of neuronal activity using light-field microscopy. *Nature methods*, *11*(7), 727–730.
- Publio, R., Oliveira, R. F., & Roque, A. C. (2006). A realistic model of rod photoreceptor for use in a retina network model. *Neurocomputing*, *69*(10-12), 1020–1024.
- Roberts, A., & Bush, B. M. (1981). *Neurons without impulses: Their significance for vertebrate and invertebrate nervous systems* (Vol. 6). Cambridge University Press.
- Rose, R., & Hindmarsh, J. (1989). The assembly of ionic currents in a thalamic neuron i. the three-dimensional model. *Proceedings of the Royal Society of London. B. Biological Sciences*, *237*(1288), 267–288.
- Sarma, G. P., Lee, C. W., Portegys, T., Ghayoomie, V., Jacobs, T., Alicea, B., Cantarelli, M., Currie, M., Gerkin, R. C., Gingell, S., et al. (2018). Openworm: Overview and recent advances in integrative biological simulation of *caenorhabditis elegans*. *Philosophical Transactions of the Royal Society B*, *373*(1758), 20170382.
- Sarpeshkar, R. (1998). Analog versus digital: Extrapolating from electronics to neurobiology. *Neural computation*, *10*(7), 1601–1638.
- Schilardi, G., & Kleinlogel, S. (2021). Two functional classes of rod bipolar cells in the healthy and degenerated optogenetically treated murine retina. *Frontiers in Cellular Neuroscience*, *15*.

- Schrödel, T., Prevedel, R., Aumayr, K., Zimmer, M., & Vaziri, A. (2013). Brain-wide 3d imaging of neuronal activity in *Caenorhabditis elegans* with sculpted light. *Nature methods*, *10*(10), 1013–1020.
- Shamir, M., & Sompolinsky, H. (2006). Implications of neuronal diversity on population coding. *Neural computation*, *18*(8), 1951–1986.
- Shiau, L., & Buhry, L. (2019). Interneuronal gamma oscillations in hippocampus via adaptive exponential integrate-and-fire neurons. *Neurocomputing*, *331*, 220–234.
- Smith, G. D., Cox, C. L., Sherman, S. M., & Rinzel, J. (2000). Fourier analysis of sinusoidally driven thalamocortical relay neurons and a minimal integrate-and-fire-or-burst model. *Journal of neurophysiology*, *83*(1), 588–610.
- Storn, R., & Price, K. (1997). Differential evolution—a simple and efficient heuristic for global optimization over continuous spaces. *Journal of global optimization*, *11*(4), 341–359.
- Strohmer, B., Stagsted, R. K., Manoonpong, P., & Larsen, L. B. (2021). Integrating non-spiking interneurons in spiking neural networks. *Frontiers in neuroscience*, *15*, 184.
- Szigeti, B., Gleeson, P., Vella, M., Khayrulin, S., Palyanov, A., Hokanson, J., Currie, M., Cantarelli, M., Idili, G., & Larson, S. (2014). Openworm: An open-science approach to modeling *Caenorhabditis elegans*. *Frontiers in computational neuroscience*, *8*, 137.
- Tsukamoto, Y., Morigiwa, K., Ueda, M., & Sterling, P. (2001). Microcircuits for night vision in mouse retina. *Journal of Neuroscience*, *21*(21), 8616–8623.
- Usui, S., Ishihaiza, A., Kamiyama, Y., & Ishii, H. (1996). Ionic current model of bipolar cells in the lower vertebrate retina. *Vision research*, *36*(24), 4069–4076.
- Werblin, F. S., & Dowling, J. E. (1969). Organization of the retina of the mudpuppy, *Necturus maculosus*. ii. intracellular recording. *Journal of neurophysiology*, *32*(3), 339–355.
- White, J. G., Southgate, E., Thomson, J. N., & Brenner, S. (1986). The structure of the nervous system of the nematode *Caenorhabditis elegans*. *Philos Trans R Soc Lond B Biol Sci*, *314*(1165), 1–340.

Wicks, S. R., Roehrig, C. J., & Rankin, C. H. (1996). A dynamic network simulation of the nematode tap withdrawal circuit: Predictions concerning synaptic function using behavioral criteria. *Journal of Neuroscience*, *16*(12), 4017–4031.